J. Fluid Mech. (1975), *vol.* 67, *part* 2, *pp.* 349–368
Printed in Great Britain

Mixing across an interface due to turbulence generated by an oscillating grid

By S. M. THOMPSON
Ministry of Works, Wellington, New Zealand

AND J. S. TURNER
Department of Applied Mathematics and Theoretical Physics,
University of Cambridge

(Received 17 July 1970 and in revised form 6 June 1974)

Many experimenters have used oscillating grids to produce turbulence for various laboratory purposes, especially in studies of mixing, but there have been few direct measurements of the properties of the turbulence itself. In the present paper we report experiments which attempt to relate the turbulent velocity and length scales to the external parameters, the frequency and amplitude, for three forms of grid oscillated in a tank of water. Turbulent velocities have been measured in the absence of a mean flow by using a hot film moved through the fluid to provide its own mean velocity. The output is stored and analysed in a small computer, which rapidly evaluates velocity and length scale statistics from an ensemble of records. The spatial variation of these quantities with distance from the stirrer is of special interest. It agrees with results suggested by an inertial-decay theory, and with previous measurements made by Bouvard & Dumas (1967) using a different form of stirrer. A particular purpose of the work has been to 'calibrate' the entrainment experiments of Turner (1968), by providing absolute scales of velocity and length in the fluid near a mixing interface, for the same grid as was used in the earlier experiments. Evidence is presented which suggests that other forms of grid may not be calibrated simply by extrapolating these results.

1. Introduction

There are many situations in nature where turbulence generated at one position in a fluid causes mixing across a density interface some distance away. For example the action of a wind on the surface of the sea is responsible for driving mixing across the seasonal thermocline, some tens of metres below, into the relatively homogeneous surface layer. For some purposes it will be necessary to consider the shear flow set up by the boundary stress, and to relate the properties of the turbulence to those of this mean flow. In other cases, however, especially when turbulence is produced on a smaller scale than the surface-layer depth (by breaking waves, for example), it is relevant to consider the one-dimensional problem of turbulence in the absence of a mean flow. The spatial

decay of turbulent energy then becomes an important consideration. Very little work has been done on this problem, however, compared with the extensive body of results for temporal decay (of turbulence behind a grid in a wind tunnel).

A few laboratory measurements of entrainment from a stationary into a turbulent layer have been reported, using stirring grids rather than a mean shear flow to produce the turbulence. Rouse & Dodu (1955) first applied this method to examine the mixing across an interface between two layers of different density, and related experiments have been reported by Cromwell (1960), Turner & Kraus (1967) and Turner (1968), among others. In all of these experiments, however, the mixing rates have been interpreted using overall measures of length and velocity scales, based on the geometry and stirring frequency. If such results are to be reproducible and more widely applicable, then one must know more about the properties of the turbulence generated in this way, and the extent to which they depend on the particular apparatus used. In this paper we describe some more detailed measurements made by Thompson (1969) in a stirred homogeneous fluid which enable us to resolve some of the uncertainties remaining after the previous experiments.

The measurements to be discussed have in fact already been used by Linden (1971) and Turner (1973) to provide quantitative estimates of turbulent velocity and length scales in the same apparatus as that used by Thompson, and a more accessible account of this work is overdue. In particular, it allows the overall results of Turner (1968) to be calibrated and reinterpreted in a more fundamental way. The results do depend more than has previously been recognized on the precise form of grid and amplitude of oscillation used; these effects, and in particular a visual study of the motions near bars of various cross-sections, are described by Thompson (1969). We shall also compare our measurements with those of Bouvard & Dumas (1967), who generated turbulence by oscillating a perforated plate in a fluid.

All our experiments were carried out in a Perspex tank of water, 254 mm square by 460 mm deep, as sketched in figure 1. This was previously used and described by Turner (1968), and reference can be made to that paper for details of the experimental arrangements. The stirring elements were mounted at mid-depth on a central spindle and oscillated vertically with frequencies between 2 and 5 Hz. For the experiments described here we used grids of horizontal bars covering the whole cross-section of the tank.

The flow produced by the oscillating grids can be discussed in terms of three consecutive processes. First, there is the generation of a quasi-steady jet flow very close to each grid bar. The form and intensity of the motion in this region depends on the cross-section of the bars and on the amplitude, and there may be an explicit dependence on viscosity. Second, the jets interact, and break down to give turbulence which is advected by the jets. Finally, this turbulence decays with distance away from the grid, in a manner which can be described using a similarity argument analogous to one which has been applied to the temporal decay of turbulence in a wind tunnel. In order to understand, say, the mixing across an interface located some distance away from an oscillated grid, one needs to know the properties of the turbulence in the region of interest, i.e. near the

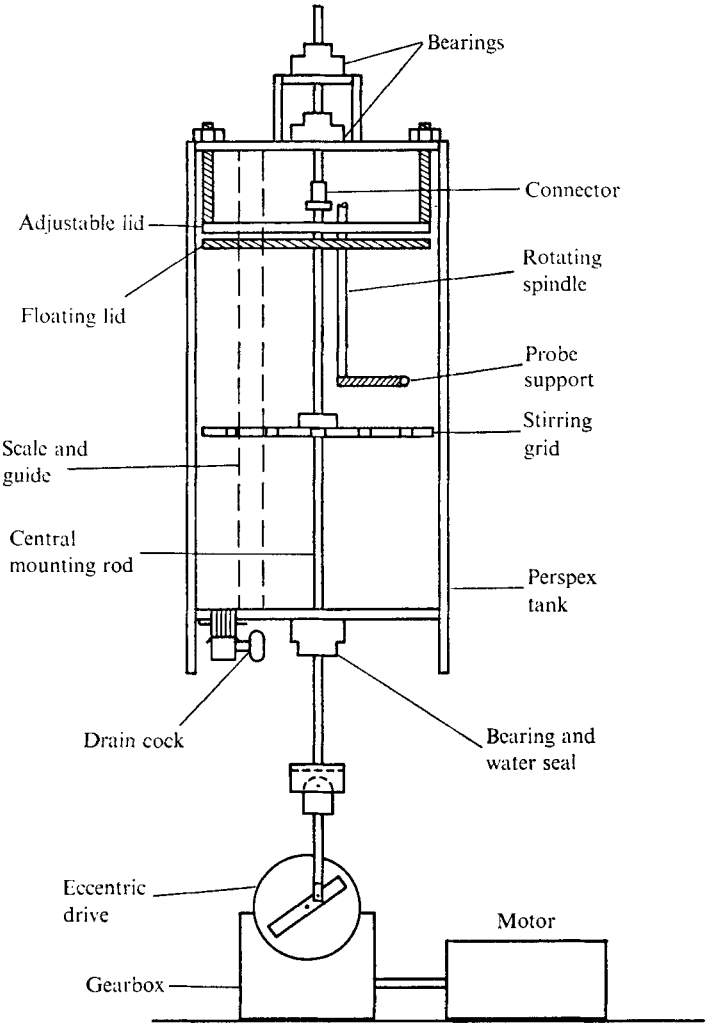

FIGURE 1. A sketch of the experimental tank, which was the same as that described by Turner (1968), slightly modified.

interface. These can be measured directly as functions of distance from the stirrer, but they will clearly depend on all of the above processes.

The fluid velocity was measured with a probe driven around a horizontal circular path at a constant speed that was much faster than the maximum fluid velocity. The fluctuation of the probe signal was interpreted as the horizontal component of velocity tangential to the circular path, and this was stored in a digital computer. After the probe had traversed nearly a complete circle it reversed back to its starting point, where it waited before the cycle was repeated. Thus many samples of the same random function were stored and analysed as a statistical ensemble. With this method of sampling it was possible to measure separately the steady eddies and the turbulent unsteady motions in a tank where the spatially averaged velocity was zero.

It is perhaps worth remarking, before we describe our own results, that chemical engineers have reported various measurements of turbulence and mixing in laboratory tanks (e.g. Moo-Young, Tichar & Dullien 1972). However, so far as we can ascertain, they have always used a rotating agitator, and the large swirling mean flows make their results hard to interpret in the present context. The less efficient kind of agitator described here is preferred because the vertical mixing it produces can be regarded as one-dimensional, and therefore more relevant for the geophysical situations we have in mind.

2. The steady flows produced by an oscillating grid

Our main concern in this paper is with the direct turbulent velocity measurements, but a brief summary of Thompson's (1969) visual observations will be helpful when it comes to interpreting the results. Streak photographs of illuminated particles led to the identification of several different flow patterns near single bars of various cross-sections, oscillated vertically with large amplitude. The most common was that shown in the photograph of figure 2(*a*) (plate 1). It consisted of a relatively slow horizontal inflow which became oscillatory near the bar and then fed fluid into strong steady vertical jets directed away from the bar. This was observed with all the shapes tested, provided that the total stroke was comparable to the width of the bar, or larger. It is qualitatively similar to the well-known steady flows generated by small amplitude oscillations of a solid body (see Batchelor 1967, p. 358; Davidson & Riley 1972), but the mechanism of generation now involves a separation of the flow past the bar. The efficiency of this kind of stirrer is consequently very low, with most of the energy put into the fluid being dissipated viscously very close to the bars.

When a grid of crossed bars is oscillated vertically with a stroke comparable to the bar diameter it generates an array of jets whose centre-lines pass through the intersection points. This is clearly demonstrated when a grid is oscillated above an erodible bed of polythene particles; provided that the grid is close enough, the bed is shaped into a regular pattern, with a hollow under each bar intersection. Further away from the grid, the regularity is lost, for two reasons. Each individual jet breaks down and becomes turbulent, by a process of shear instability at its edges, and there is also an interaction between the jets. Using bars of circular cross-section, for instance, the presence of the individual jet flows is still detectable on streak photographs up to a distance of about twice the spacing, but beyond that they have merged to form an irregular turbulent flow.

A flat grid of square bars with 50 mm spacing, oscillated with a stroke of 10 mm (equal to the side of the square cross-section), turned out to be a rather special case. No clear jets were visible on streak photographs even quite close to the grid (see figure 2*b*), and the flow appeared to break down rapidly to a confused turbulent state. Since this was the form of grid used by Turner (1968) it has been used also for many of the measurements reported in this paper, and it is important to appreciate how the turbulence produced by it may differ from that produced by grids used by other experimenters.

Even for these bars of square cross-section, however, the detailed velocity measurements (such as those illustrated in figure 4) indicate that steady flow patterns can be detected in all parts of the tank. These are associated with the grid geometry up to 80 mm from the grid, but lose this association at greater distances. This implies again that the jet flows remain distinct for about two mesh lengths, then combine in a pattern which is determined by the shape of the tank, and by small differences in the strength of the flow from different parts of the grid.

It is possible that the action of a stirring grid in a tank (in producing mixing across a density interface, for example) may depend essentially on the steady component of the flow as well as on the turbulence. If so, such measurements would be very specific to the particular apparatus, and not easily transferred to other situations. We shall show in the following, however, that the unsteady turbulent motions did make the dominant contribution to the measured velocities in our tank, and that it is therefore reasonable to make more general deductions from particular measurements, provided that they are made not too close to or far away from the stirring grids.

3. The technique of turbulent velocity measurements

The measurement of turbulence in the absence of a mean flow poses special problems. In order to provide a steady non-reversing flow on which the fluctuations were superimposed, a hot-film probe was attached to a rotating vertical spindle so that its tip traversed a circular horizontal path of radius 70 mm at 100 mm/s, in a plane parallel to the grid and at an adjustable distance from it. (Figure 3 (plate 1) shows the probe in position in the tank.) The probe therefore sampled the *horizontal* velocity, not the vertical motions observed by the streak technique. It was stopped just before it completed a revolution, and then reversed back to its starting point, so that no net circulation was imparted to the fluid, and it did not sample its own wake. The probe was kept stationary for at least 25 s between samples.

The tip of the probe rapidly became contaminated by bubbles and small particles in a way that reduced its sensitivity, and it was necessary to clean it frequently. This was done using two fine water-colour paint brushes, the probe tip passing between them before the start of each sampling sweep. The probe was driven at constant speed by a wire passing round pulleys to a falling weight, with one pulley attached to a mechanical governor. The probe accelerated over 50 mm, sampled over 254 mm, then decelerated over 20 mm of its travel. Calibration was performed *in situ* by comparing a signal obtained in still water with one recorded when the probe passed 10 mm below the tip of a vertical tube, 5 mm in diameter, through which a known flow was being withdrawn. With this arrangement, the velocity field traversed by the probe approximated closely to that due to a sink of known strength situated at the centre of the tip of the tube, which was easily calculated for comparison with the probe signal. The calibration was effectively linear over the range of velocities measured.

The signal from the probe was recorded and analysed using a system which included the following devices, operated on-line and in real time:

(*a*) DISA 55A85 quartz-coated platinum film probe on a quartz wedge;

(*b*) DISA 55A01 constant-temperature probe circuit;

(*c*) Systems Computers TAG30 analog computer incorporating operational amplifier circuits;

(*d*) Digital Equipment Corporation PDP8 digital computer incorporating an analog–digital converter and disc memory;

(*e*) Telequipment D53 oscilloscope display.

A short sample of turbulent velocity was obtained with each sweep of the probe. Each sample was a function of both time and space, but since the speed of the probe was much faster than the measured velocities, and the radius of its path was much greater than the integral scale of the turbulence, the sample was interpreted simply as a function of a single spatial co-ordinate. The signal was digitized every 2 mm and stored as 128 values per sample. Successive samples consisted of measurements at the same 128 points in space, so that ensemble statistics could be calculated for the data at these points.

The data analysis, which was carried out immediately as the experiment proceeded, was arranged so that the ensemble of the first half of the samples was compared with the ensemble of the last half. A calibration made before a run was also compared with a calibration afterwards. When these checks detected malfunction of the probe system, or unsteadiness of the 'mean flow' in the box, the samples were discarded and the cause sought and remedied. Once measurements on a particular flow were found to be reproducible from day to day, the result was accepted.

The autocovariance of the turbulent velocity was estimated from ensembles of 16 or more samples as follows. Let $W_{n,x}$ represent the basic voltage data, where n is the ensemble number, usually with a range 1–16, and x is the distance along the sample, expressed in units of 2 mm (and therefore with a range 1–128) The turbulent velocity V was calculated as

$$V_{n,x} = (\text{scaling factor}) \left(W_{n,x} - \frac{1}{128} \sum_{x=1}^{128} W_{n,x} \right). \tag{1}$$

The ensemble-mean velocity at a point is

$$\overline{V}_x = \frac{1}{16} \sum_{n=1}^{16} V_{n,x}, \tag{2}$$

and the ensemble-mean autocovariance of the samples is

$$B_y = \frac{1}{16(128-y)} \sum_{n=1}^{16} \sum_{x=1}^{128-y} V_{n,x} V_{n,x+y}, \tag{3}$$

where y is the lag measured in the same units as x. This was calculated for all values of y between 0 and 48.

The records obtained by the above method were in fact too short for (3) to give an accurate estimate of the autocovariance. There were slower fluctuations of velocity in the stirred box, which led to the individual sample means

being displaced by unknown amounts from the true mean, with a variance that was a significant fraction of the variance of the record. This is indicated by the small negative values of the autocovariance persisting at large lags (as illustrated in the examples shown in figure 4). The procedure used for correcting for this effect is described in detail in the appendix, but for the present we just state the result. An improved estimate of the true autocovariance A_y is obtained from B_y thus:

$$A_y = B_y + \frac{1}{24} \sum_{y=25}^{48} B_y. \tag{4}$$

Finally, a velocity scale u of the turbulence is defined as the root mean square:

$$u = A_0^{\frac{1}{2}} \quad \text{(mm/s)}. \tag{5}$$

A length scale l is defined as the normalized area under the autocovariance curve:

$$l = \left(1 + 2 \sum_{y=1}^{24} A_y/A_0\right) \quad \text{(mm)}. \tag{6}$$

The physical dimension in (6) is set by the 2 mm spacing between the points at which the velocity was digitized.

4. Examples of velocity records

Some examples of records analysed by the method described are shown in figure 4 for the experiments listed in table 1. They were obtained by displaying the stored digital records on an oscilloscope screen, and photographing them. The first eight photographs of each set are individual velocity records, and they are followed by four ensemble averages, as defined by either (2) or (3). The numbers on the velocity records and the mean velocities are the r.m.s. velocities in mm/s, and the numbers on the autocovariances are the integral length scales in mm. The abscissa scale of the velocity records is twice that of the autocovariances, and every second point on the latter is not shown. Thus the velocity records show 128 points representing 256 mm, and the autocovariances show only 24 points representing 96 mm in the direction of motion of the probe. The tops of the autocovariances in figures 4(*b*)–(*d*) have been cut off, so that the points for zero and 4 mm lags are not shown, but, although it is not evident from the figure, all autocovariances had the same sharp maximum at zero lag, as in figure 4(*a*).

The first set of records (figure 4*a*) illustrates results with the measuring system in its most sensitive range. The first two ensembles in the third row are the mean velocity and autocovariance of the 8 velocity records reproduced above them. The second pair are the same functions calculated from an ensemble of 32 velocity records which included the 8 illustrated; these are a little smoother, but very similar to the first pair.

The set in figure 4(*b*) was obtained in conditions where the r.m.s. velocity was larger, but using a less sensitive range. The first two ensembles are the mean velocity and autocovariance of a set of 16 velocity records. The third trace in the

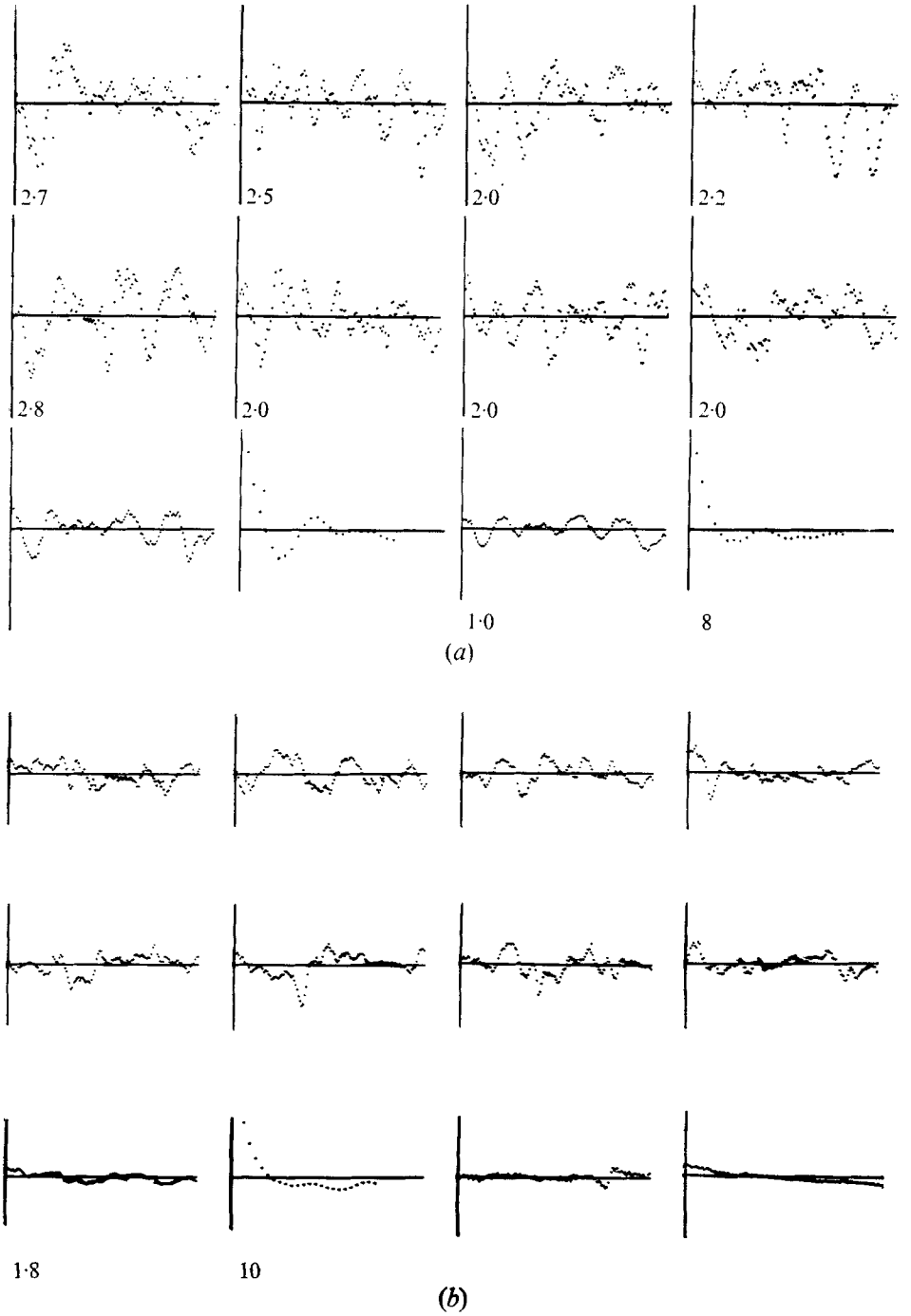

FIGURES 4(*a*, *b*). For legend see facing page.

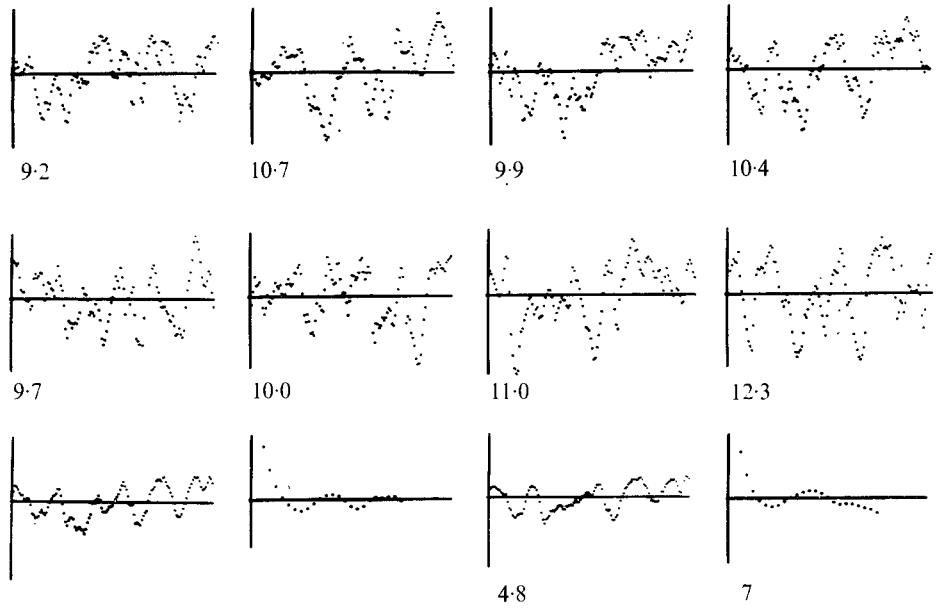

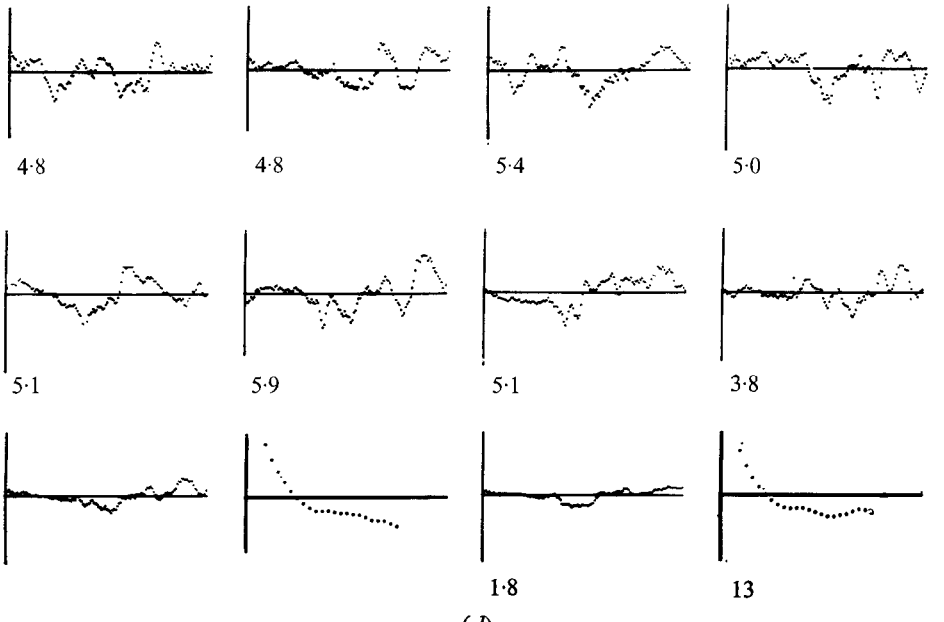

FIGURE 4. Examples of records of the horizontal turbulent velocity obtained using a hot-film probe in a tank of water stirred by an oscillating grid. A description of the flows measured and of the particular data illustrated is given in table 1, and more detail is to be found in § 3.

Stirring grid	(*a*)	(*b*)	(*c*)	(*d*)
Bar shape	Square	Round	Round	Round
Bar width (mm)	10	9·52	9·52	9·52
Mesh (mm)	50	50	50	50
Frequency, f (Hz)	3·33	2·78	5·0	5·0
Stroke, s (mm)	10	14·5	14	14
Flow				
Distance from grid, z (mm)	70	90	70	130
Length scale, l (mm)	8	10	7	14
Velocity scale, u (mm/s)	2·4	4·3	9·5	4·9

TABLE 1. The conditions used, and the results obtained, in the experiments corresponding to the records shown in figure 4

third row is a calibration record, in which the trough and peak represent a velocity excursion from -5 to $+5$ mm/s. The irregular oscillations at the left indicate r.m.s. 'noise' of 1 mm/s, which was subtracted from all of the estimates of r.m.s. velocity. The last trace is the ensemble mean of many records obtained in still water, which has been applied as a correction to all the velocity records in this set. Its cause is unknown, but it varied from day to day rather than hour to hour, and could be repeated before and after a run. Frequently it was zero (as one might expect *a priori*), and it was seldom as large as in the case illustrated.

The last two sets of 12 records (figures 4*c*, *d*) illustrate how the velocity varies with distance from the stirrer in the same flow (a topic which will be discussed in more detail in §5). The first two ensembles in each case are the mean velocity and autocovariance of the 8 velocity records illustrated, and the second pair are the same functions calculated from a set of 24 velocity records. Note that the ensemble-mean velocities indicate the presence of quasi-steady flow patterns in all parts of the tank, i.e. the mean velocities are significantly different from zero even at three mesh lengths from the grid and beyond. Let us define a velocity scale for these steady flows as

$$U = \left(\frac{1}{128}\sum_{x=1}^{128}\overline{V}_x^2\right)^{\frac{1}{2}}. \tag{7}$$

In table 2 we have compared this quantity with the total r.m.s. velocity u measured at various distances from the grid in the experiment described in table 1, columns (*c*, *d*). There was clearly no systematic variation of U/u with distance, and the mean value was about 0·43. Thus the r.m.s. unsteady velocity u_1, defined by

$$u^2 = u_1^2 + U^2, \tag{8}$$

was approximately $u_1 = 0{\cdot}9u$, rather larger than U. (We should remember that the measured velocities are all horizontal, and are not directly related to the vertical velocity in individual jets observed near the grid.)

Distance from grid, z (mm)	50	60	70	80	90	110	130	130	150	150	170
No. of records in ensemble	16	24	24	16	16	16	24	16	24	16	16
u (mm/s)	13·0	11·3	10·2	9·5	7·7	6·2	4·9	4·9	3·8	3·8	2·7
U/u	0·51	0·49	0·43	0·41	0·43	0·57	0·38	0·42	0·42	0·46	0·31

TABLE 2. A comparison of the r.m.s. steady velocity, calculated according to (7), with the total r.m.s. velocity u at various distances from the grid for the flow described in table 1(c, d)

The relation between the steady component of the flow at various levels and the geometry of the grid below is shown on figure 5 for this same experiment. A plan of the grid is superimposed on the path of the probe, with arrows indicating the direction of the ensemble-mean velocity (i.e. the steady flow). It can be seen that this direction remains associated with the grid bars up to 80 mm from the grid, but not at the two larger distances shown.

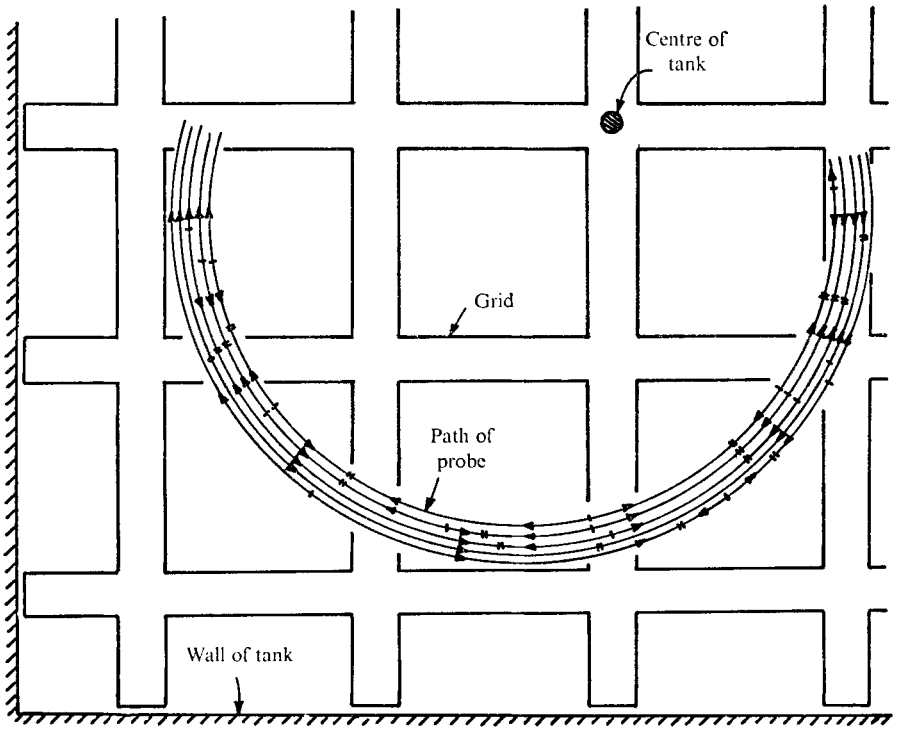

FIGURE 5. A plan view, showing the path of the hot-film velocity probe in relation to the grid stirrer below it, with arrows indicating the direction of the ensemble-mean velocity along this path. Data are shown for five distances from the grid for the experiment described in table 1(c) and table 2. For clarity the paths are displaced, with the circles from inner to outer representing the measurements at z = 50, 60, 80, 110 and 130 mm respectively, but all of them were actually made vertically above one another at a radius of 70 mm.

5. The spatial decay of turbulence

We now turn to the question of the variation of turbulent velocity and length scales with distance from the energy source. As we have indicated in the introduction, this problem is important in various geophysical applications, but relatively little attention has been given to it, compared with that of temporal decay (of turbulence generated by a fixed grid in a wind tunnel). In order to provide a framework in which to present our measurements, some simple arguments based on dimensional considerations will first be outlined. They are related to a 'diffusion of turbulent energy' argument proposed by Bouvard & Dumas (1967) (whose measurements are compared with ours below) and to that used to describe the temporal decay of turbulence at high Reynolds numbers.

In the latter case, the time rate of change of energy in homogeneous turbulence can be expressed as (Batchelor 1953, p. 113)

$$du^2/dt = -Au^3/l, \tag{9}$$

where u and l have similar meanings to those defined above and A is a constant of order one. This implies, quoting Batchelor, "that an eddy viscosity of order ul is acting on a shear of order u/l to produce a 'dissipation' of energy from the energy-containing eddies to smaller eddies". Note, however, that an *inertial* transfer process is the dominant one here, and molecular viscosity does not enter directly.

In the same way, it is proposed, the variation with distance z of turbulence which is continuously generated by an oscillating horizontal grid at $z = 0$, and is steady in time and homogeneous in horizontal planes, can be described by

$$du^3/dz = -Bu^3/l. \tag{10}$$

The left-hand side is the divergence of the flux of turbulent energy and (10) expresses the fact that the inertial 'dissipation' process now acts to reduce this energy flux across successive horizontal planes.

Anticipating the experimental results, let us now consider a linear variation of l with z:

$$l = \beta z. \tag{11}$$

It follows from (10) that the corresponding turbulent velocity will have a power-law dependence on z:

$$u = u_0 (z/z_0)^{-B/3\beta}, \tag{12}$$

where the distance has been made dimensionless with the length scale z_0 and u_0 is a measure of the velocity at $z = z_0$. A more definite proposal about the choice of z_0 is made in the following section.

Measurements supporting the relations (10)–(12) have already been reported by Bouvard & Dumas (1967), who oscillated a horizontal plate 40 mm thick, perforated with 45 mm diameter holes, near the bottom of a tank 675 mm square, and measured the decay of turbulence using techniques similar to those described in this paper. Their results will be described first, since their larger tank and more

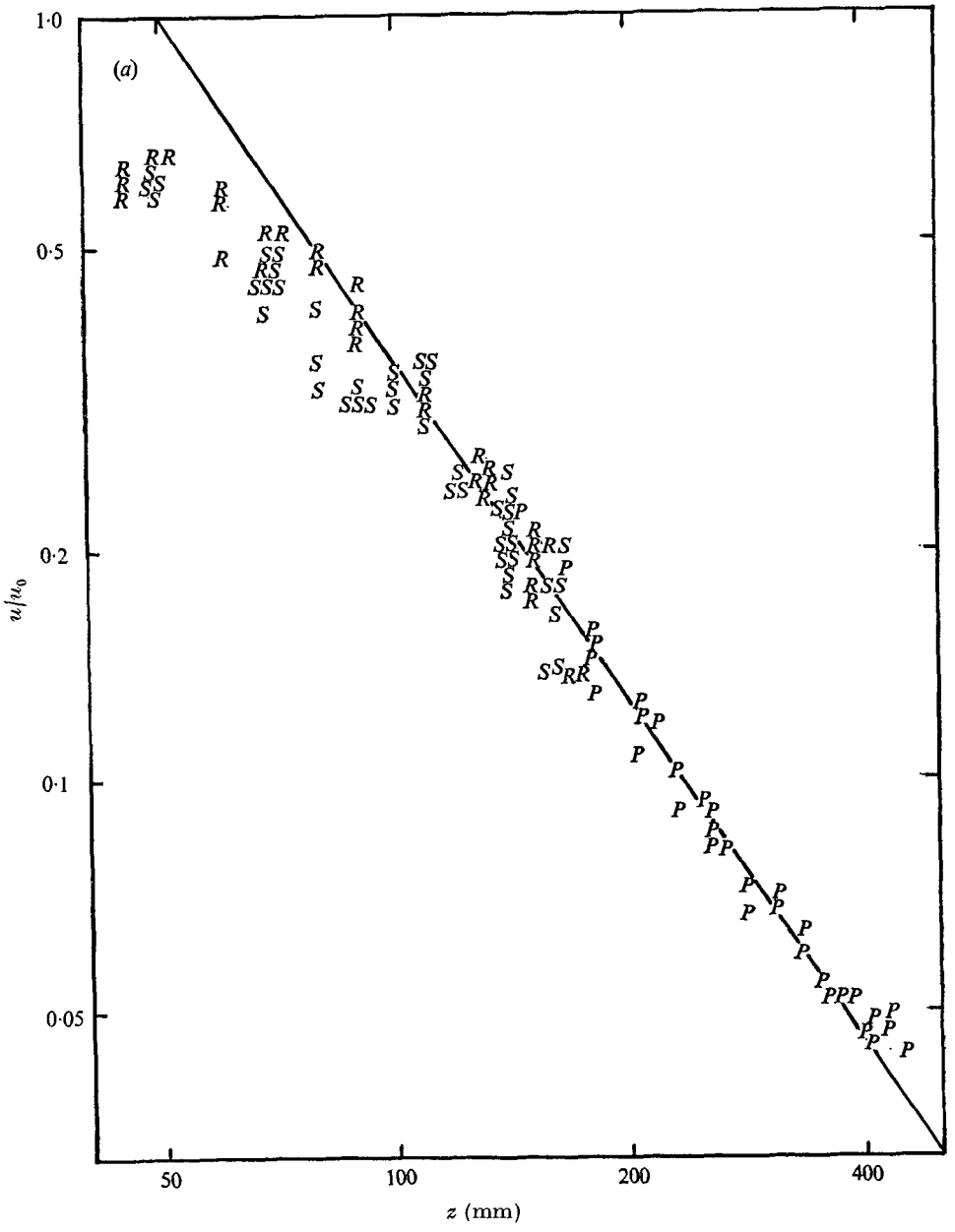

FIGURE 6(*a*). For legend see next page.

vigorous stirring (at 6 Hz with a stroke of 80 mm) gave Reynolds numbers ul/ν ranging up to about 3000, at which the inertial-decay theory is most likely to be valid. Our grid measurements (with $ul/\nu \approx 50$) are also, however, consistent with the same hypotheses.

The data points marked P on figure 6 represent the perforated-plate results, actually replotted from figures IV 4 and 10 in Bouvard's thesis, which are

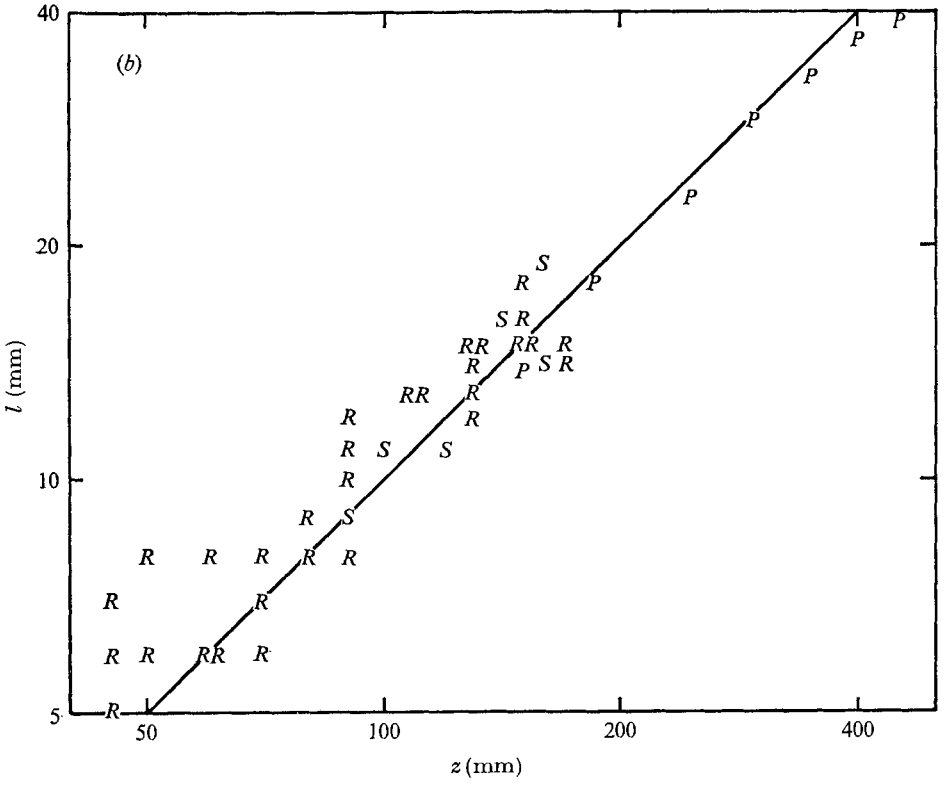

FIGURE 6. (*a*) Root-mean-square horizontal velocity u, plotted logarithmically against distance z from the stirrer for comparison with (12). Each S point and R point represents an ensemble of 8 velocity records. S, square-bar grid in table 1 (*a*); the velocity scale corresponding to $z_0 = 50$ mm is $u_0 = 8$ mm/s; R, round-bar grid in table 1 (*c*), $u_0 = 20$ mm/s; P, perforated plate used by Bouvard & Dumas (1967), $u_0 = 1500$ mm/s. (*b*) Integral length scale l of the horizontal spatial covariance of the horizontal velocity u, plotted logarithmically against z for comparison with (11). The notation is the same as that used in (*a*). Each S point represents at least 24 velocity records and each R point at least 8 velocity records.

reproduced on a smaller scale in Bouvard & Dumas (1967). The distances z are measured from the mean position of the plate, and the velocities are scaled with the value u_0 at a fixed position, arbitrarily chosen as $z_0 = 50$ mm. The slopes of the lines drawn on figure 6 are consistent with $B = 0{\cdot}45$, $\beta = 0{\cdot}10$ and $u \propto z^{-1{\cdot}5}$.

Also plotted on figure 6 are data from the grid experiments described in §§3 and 4 of the present paper. The results for square bars (used under the conditions detailed in table 1 (*a*)) are denoted by S, and those for round bars (table 1(*c*)) by R. In these cases a 'virtual origin' for z has been chosen to maximize the agreement with (11) and (12); the displacements (behind the grids) are 10 mm for S and 20 mm for R. At distances sufficiently far from the stirrer, the *same* relations (10)–(12) can be used to describe the variations of the length and velocity scales of the turbulent motion, i.e. the same power laws apply. In order to bring all the results onto the same line in figure 6 (*a*) a different value of u_0 must be chosen for

each experiment (as listed in the caption), to take account of the different rates of energy generation by each stirrer. Up to $z = 80$ mm the spatial decay of u shown on figure 6(*a*) for the grid-generated turbulence is less rapid than $r^{-1.5}$, and this is presumably due to a significant generation of turbulence in this region, associated with the jet motions discussed in conjunction with figure 5.

Bouvard & Dumas' results also show that there is a region of slightly increased horizontal turbulent velocity near a free surface, due to the proximity of the horizontal boundary. At very large distances from the grid, direct viscous effects, rather than the inertial transfer mechanism assumed here, must become dominant; but further study of these processes lies outside the scope of the present investigation.

6. The relation between turbulent velocity and stirring frequency

We have also explored the effects of varying other quantities, besides the distance, on the turbulence measurements described in §3. We hoped to be able to relate the turbulent energy generation (and hence u_0) to the external parameters such as frequency, stroke and grid geometry, but the results are very complicated and we can report only limited success. In particular the frequency (f) dependence will be discussed here for experiments using two kinds of grids.

In figure 7, the points (*a*) are measurements made using a grid of square bars, under the conditions described in table 1 (*a*) (except that the frequency was varied). To good accuracy we can write $u \propto f$ (at a fixed distance from the square bars, and using a fixed stroke of 10 mm). Though we cannot support this further step with detailed velocity measurements, the cruder results obtained from streak photographs (see §2) suggest that we can write $u_0 \propto fs$, where s is the stroke. This assumption, which implies that the turbulent velocity is proportional to the maximum velocity of the grid, is also attractive physically. For round bars, on the other hand, the measurements (made under the conditions in table 1 (*b*)) are the form shown by the line (*b*) in figure 7. This indicates a different dependence on frequency, $u \propto f^{\frac{4}{3}}$ approximately, which is only possible dimensionally if some other physical quantity containing the dimensions of time enters into the expression for the velocity. The neglected factor, we suggest, must be the viscosity ν. For some grid cross-sections, including round bars, viscosity must be invoked explicitly before we can fully understand what determines the velocity scale u_0 in (12).

Always bearing the above uncertainties in mind, it is of interest to record two results which may be a useful guide to those planning further experiments of this type. The data on figures 6(*a*) and 7, regardless of the form of stirrer, are described to within 50 % by the dimensionally consistent equation

$$u = 1{\cdot}4 f s^{2{\cdot}5} z^{-1{\cdot}5}, \tag{13}$$

which is obtained from (12) by putting $u_0 \propto fs$ and using s as the length scale z_0. The Reynolds number of the turbulence is, from (11) and (13),

$$ul/\nu = 0{\cdot}14 f s^{2{\cdot}5}/\nu z^{0{\cdot}5}. \tag{14}$$

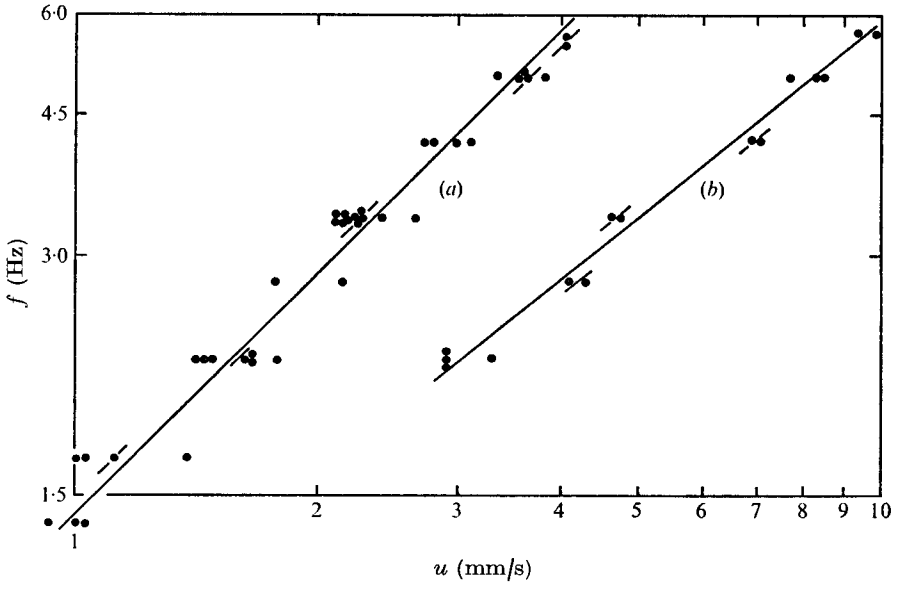

FIGURE 7. (*a*) Root-mean-square horizontal velocity u at $z = 70$ mm, plotted logarithmically against grid oscillation frequency f. The stirrer was the square-bar grid described in table 1 (*a*), oscillating with stroke $s = 10$ mm, and each point represents an ensemble of 8 records. (*b*) Root-mean-square horizontal velocity u at $z = 90$ mm, plotted logarithmically against frequency for the round-bar grid described in table 1 (*b*).

This decreases slowly with increasing distance from the grid even in the 'inertial' range.

We are now in a position to complete one of the main aims of this study, the 'calibration' of Turner's (1968) mixing experiments (as discussed in the introduction). Those experiments and the present set were carried out in the same tank, using the identical grid of square bars over the same range of conditions. On the assumption that the flow of the uniformly dense fluid near the grid was the same in both cases, the details of the turbulent flow adjacent to the stable interfaces can now be inferred from the known parameters of the grid motion.

The effective velocity and length scales of the turbulence acting on Turner's interfaces are taken to be the values measured at $z = 90$ mm. This is one length scale nearer to the grid than the average level of the interface. (The grid–interface distance used was actually 90 mm, but allowance has also been made for the shift in the origin of z, which was 10 mm for square bars.) Combining the data on figures 6 (*a*) and 7 (*a*) which relate to square bars, we find that, for $f = 5$ Hz and $z = 90$ mm, $u = 2{\cdot}8$ mm/s; so that

$$u = 0{\cdot}56f \text{ mm/s}. \tag{15}$$

From figure 6 (*b*), at $z = 90$ mm, $l = 9$ mm. (16)

Turner (1968) used arbitrary scales, defined in terms of a stirring frequency n and the fixed (but unknown) length scales, to plot (in his figure 3) entrainment rates against a stability parameter which was proportional to a Richardson number. We now seek non-dimensional forms of these parameters, based on u

and l. The scaling factor by which the previous ordinate u_e/n (in units of cm/cycle) must be multiplied to convert it to u_e/u as defined by (15) is 17·8. The corresponding factor for the abscissa, required to convert the arbitrary $3 \times 10^8 \Delta\rho/\rho n^2$ (where n was expressed in cycles/min) to $Ri_0 = g\Delta\rho l/\rho u^2$ using (15) and (16), is 3·4. These are the factors used by Turner (1973, p. 291) to replot the 1968 data in a more fundamental way, incorporating the flow parameters u and l.

In conclusion, we should emphasize again that this straightforward conversion of scales has only been possible because of the *linear* relation (15) between turbulent velocity and stirring frequency. It was fortunate for this purpose that the bars of square cross-section behaved in this way, so that the stirring frequency gave a genuine measure of the *fluid* velocities, as had previously been assumed. But our results also contain the warning that, with other shapes of grid, the determination of the relevant fluid velocity need not be so simple. Viscous effects, which have been attributed to processes occurring near an entraining interface, may in fact arise very near the stirring grid. Provided that a velocity scale can be found by direct measurement in the fluid, however, the results of §5 give us confidence that the turbulence produced by a variety of forms of stirrer, in a region of zero mean velocity, has a universal character which will make it a useful experimental tool.

The experiments reported here were carried out in the Department of Applied Mathematics and Theoretical Physics, Cambridge, while S. M. T. was a student there, and he is grateful to the New Zealand Ministry of Works for financial support during that period. We also acknowledge the support of a grant from the British Admiralty, the guidance of J. W. Elder and P. Moore in the use of their newly developed hybrid computer system, and the suggestion of A. A. Townsend about estimating the autocovariance, as described in the appendix.

Appendix

When estimating the autocovariance of a random record from a set of 'short' samples, it may be possible to correct for an error that arises when the sample means are displaced by unknown amounts from the true mean. In this context a sample is regarded as 'short' when the variance of the displacement of its mean is a significant fraction of the variance of the record.

The correction defined in (4) was possible because the autocovariances calculated by (3) apparently approached asymptotically a small negative constant at large lags. The following explanation was suggested by Dr A. A. Townsend (private communication), and we understand that he used the correction in the work he reported in Townsend (1970, p. 31).

Consider a record consisting of non-intersecting rectangular pulses distributed randomly in terms of an independent variable x, with positive and negative signs occurring equally often so that the mean is zero. Also suppose that this record is obtained by superimposing two simpler records f_x and F_x, in each of which all the pulses are of the same kind:

(*a*) f_x consists of pulses of height h and width w at an average spacing of s;

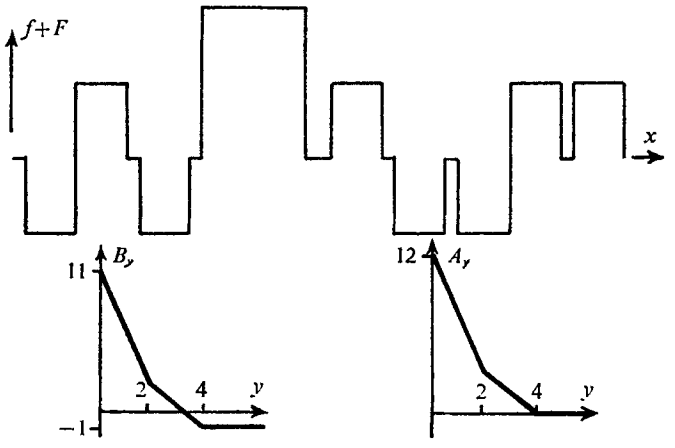

FIGURE 8. A sample of a random record constructed from two kinds of rectangular pulses, as described in the appendix. The relative magnitudes of h, w, s and H, W, S are 3, 2, 3 and 6, 4, 24 units respectively. The sketches below are the corresponding uncorrected and corrected autocovariances B_y and A_y.

(*b*) F_x consists of pulses of height H and width W at a larger average spacing of $S \gg s$.

Figure 8 shows what such a record might look like, and the form of the corresponding autocorrelation function, as calculated below.

A sample of length $R \gg S$ will have a mean close to the true mean and the expected autocovariance is

$$A_y = \frac{1}{R-y}\int_0^{R-y} (f_x + F_x)(f_{x+y} + F_{x+y})\,dx \tag{A 1}$$

$$= \frac{1}{R-y}\int_0^{R-y} f_x f_{x+y}\,dx + \frac{1}{R-y}\int_0^{R-y} F_x F_{x+y}\,dx \tag{A 2}$$

$$= \frac{1}{s}\int_0^{w-y} h^2\,dx + \frac{1}{S}\int_0^{W-y} H^2\,dx \tag{A 3}$$

$$= \{w-y\}h^2/s + \{W-y\}H^2/S. \tag{A 4}$$

A convention is adopted here that the curly-bracketed terms are zero when the enclosed expression is negative. Equation (A 1) is equivalent to (4), equation (A 2) follows because f_x and F_x are uncorrelated, (A 3) because the contributions from pulses of the same shape are all the same, and (A 4) by integration of (A 3).

However a 'short' sample of length S is expected to have just one pulse from F_x. Thus for $y \ll S$ and $s \ll S$ we have the following expected values:

$$\frac{1}{S-y}\int_0^{S-y} F_x\,dx = \frac{1}{S-y}\int_0^{S-y} F_{x+y}\,dx = HW/S, \tag{A 5}$$

$$\frac{1}{S-y}\int_0^{S-y} f_x\,dx = \frac{1}{S-y}\int_0^{S-y} f_{x+y}\,dx = 0, \tag{A 6}$$

so that the sample mean is displaced a height of HW/S from the true mean. The effect of this is that the expected sample autocovariance is

$$B_y = \frac{1}{S-y}\int_0^{S-y} (f_x + F_x - HW/S)(f_{x+y} + F_{x+y} - HW/S)\,dx \tag{A 7}$$

$$= \frac{1}{S-y}\int_0^{S-y} f_x f_{x+y}\,dx + \frac{1}{S-y}\int_0^{S-y} F_x F_{x+y}\,dx$$

$$- 2(HW/S)\frac{1}{S-y}\int_0^{S-y} F_x\,dx + (HW/S)^2 \tag{A 8}$$

$$= \{w-y\}h^2/s + \{W-y\}H^2/S - (HW/S)^2. \tag{A 9}$$

To obtain the true autocovariance [A_y, defined in (A 4)] we must add $(HW/S)^2$ to B_y, and the value of $(HW/S)^2$ will be the observed constant magnitude of B_y at lags larger than w and W.

The assumptions of non-intersecting rectangular shapes and two kinds of pulse simplified this presentation; but these assumptions are believed to be much more restrictive than is strictly necessary for the result of the previous paragraph to hold, and the argument can be generalized. A record of turbulence may usually be interpreted as the sum of pulses of many sizes, shapes and spacings, each turbulent eddy contributing a pulse as it passes the probe. It is plausible that the spacing of pulses of a particular 'kind' should be larger than their width. The autocovariances in figures 4(*a*) and (*c*) indicate that, at about 70 mm from the grid, the largest pulses had a width of 25 mm and that roughly 5 % of the variance is from pulses spaced about 250 mm (the length of the sample) apart.

Negative autocovariances will also arise when there is a trend, or regular oscillations, in the ensemble mean. There is some evidence of both these effects on figure 4 in addition to the approach to a negative autocovariance at large lags. Tests were made in which the autocovariance of the ensemble mean was subtracted from the ensemble autocovariance discussed above, but this correction did not significantly affect the estimates of the velocity and length scales u and l.

REFERENCES

Batchelor, G. K. 1953 *Homogeneous Turbulence.* Cambridge University Press.

Batchelor, G. K. 1967 *An Introduction to Fluid Dynamics.* Cambridge University Press.

Bouvard, M. & Dumas, H. 1967 Application de la méthode de fil chaud à la mesure de la turbulence dans l'eau. *Houille Blanche*, **22**, 257, 723.

Cromwell, T. 1960 Pycnoclines created by mixing in an aquarium tank. *J. Mar. Res.* **18**, 73.

Davidson, B. J. & Riley, N. 1972 Jets induced by oscillatory motion. *J. Fluid Mech.* **53**, 287.

Linden, P. F. 1971 Salt fingers in the presence of grid-generated turbulence. *J. Fluid Mech.* **49**, 611.

Moo-Young, M., Tichar, K. & Dullien, F. A. L. 1972 The blending efficiencies of some impellors in batch mixing. *A.I.Ch.E. J.* **18**, 178.

Rouse, H. & Dodu, J. 1955 Diffusion turbulente à travers une discontinuité de densité. *Houille Blanche*, **10**, 522.

THOMPSON, S. M. 1969 Turbulent interfaces generated by an oscillating grid in a stably stratified fluid. Ph.D. thesis, University of Cambridge.

TOWNSEND, A. A. 1970 Entrainment and the structure of turbulent flow. *J. Fluid Mech.* **41**, 13.

TURNER, J. S. 1968 The influence of molecular diffusivity on turbulent entrainment across a density interface. *J. Fluid Mech.* **23**, 639.

TURNER, J. S. 1973 *Buoyancy Effects in Fluids.* Cambridge University Press.

TURNER, J. S. & KRAUS, E. B. 1967 A one-dimensional model of the seasonal thermocline I. A laboratory model and its interpretation. *Tellus*, **19**, 88.

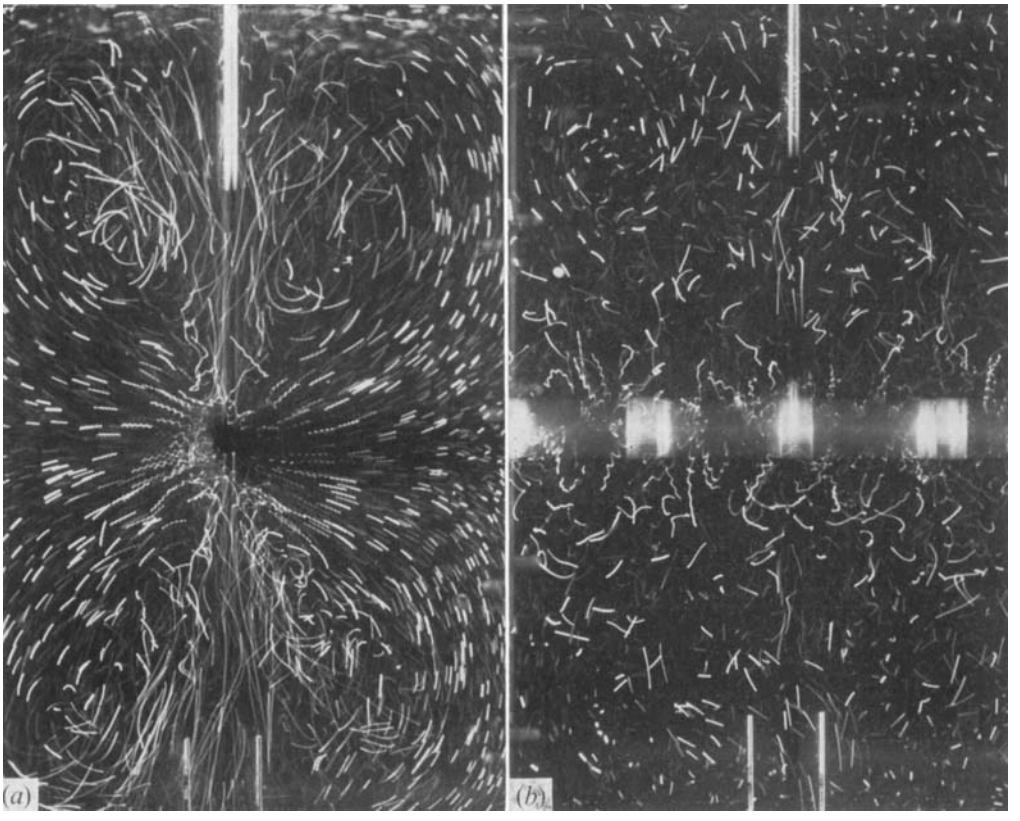

FIGURE 2. Streak photograph of neutrally buoyant polythene balls, illuminated through a vertical slit at right angles to the line of sight: exposure time, 1 s. The pins at the bottom of the pictures were 2·5 cm apart. (*a*) Nearly two-dimensional vertical jet flows generated above and below a single cylinder oscillating vertically with its axis horizontal. The cross-section was a 12·7 mm square on edge, oscillated parallel to a diagonal with frequency 5 Hz and stroke 10 mm. (*b*) A three-dimensional turbulent flow about a grid stirrer with square cross-section. Measurements of this flow are shown on figure 6 with the symbols *S*, and on figure 7 (*a*).

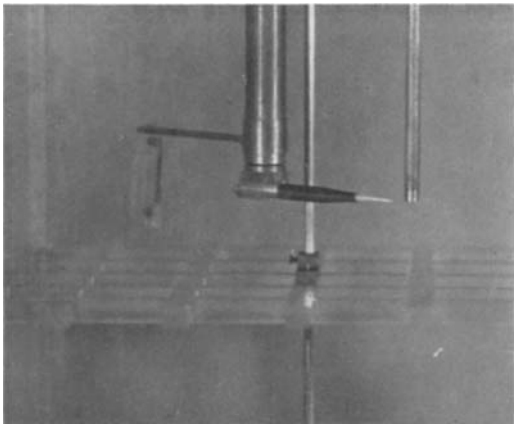

FIGURE 3. A photograph showing the hot-film velocity probe, mounted in the tank above one of the grid stirrers. From the left can be seen (*a*) the brushes which cleaned the tip of the probe; (*b*) the probe support; (*c*) the central grid support; and (*d*) the tube through which fluid could be withdrawn to create a known flow in an otherwise still tank for calibrating the probe's response.